PROCEEDINGS of the
23rd International Congress on Acoustics

9 to 13 September 2019 in Aachen, Germany

Numerical Analysis of the Nonlinear Restoring Force Based on Near-field Acoustic Levitation

Yuanyuan LIU[1]; Minghui SHI[2]; Kheirollah SEPAHVAND[1]; Steffen MARBURG[1]

[1] Department of Mechanical Engineering, Technical University of Munich, 85748 Garching, Germany

[2] College of Mechanical and Vehicle Engineering, Hunan University, 410082 Changsha, China

ABSTRACT

The stability of the floating object is a key factor in near-field acoustic levitation, which has an extensive application prospect in manufacturing of micro-electromechanical system parts. This study presents a numerical study of the restoring force based on the theory of gas film lubrication. Finite difference scheme is used to solve the Reynolds equation considering the movement of reflector and to obtain the air pressure distribution. After coordinate transformation, the restoring force which acts on the levitator can be acquired. An experimental rig is constructed to measure the restoring force with different eccentricity. The experimental results show that the restoring force increases with the increase of eccentricity. The numerical results match well with experimental results.

Keywords: Acoustic levitation; Eccentricity; Restoring force

1. INTRODUCTION

Recently, near-field acoustic levitation (NFAL) technology has been rapidly developed. Comparing with the traditional non-contact levitation technology, such as air cushion (1) and magnetic system (2), NFAL system is a very compact system, which don't need an additional air compressor to provide high pressure air and don't produce an undesirable magnetic field. However, the manufacture and installation error will produce the acoustic viscous force caused by the gradient of the sound field in the fluid, which will affect the stability of floating object (3). Owing to the existence of the viscous force, if the floating object has a little eccentricity, it will push the object toward center, which is also called restoring force. In 2000, Koike *et. al* (4) used the block-spring model to evaluate the stability and calculated acoustic viscous forces in two direction based on the theory of the near-boundary acoustic streaming. Li *et. al* (5) pointed out that the block-spring system model can only treat small amplitude oscillation because of its linear approximation. They used Stokes micro-continuum theory and acoustic radiation potential method to solve the restoring force. However, the corresponding experimental results were not given in that paper.

This paper introduces a suggested method to acquire the restoring force when centers between radiator plate and reflector plate are misaligned. At first, an updated Reynolds Equation which considering the movement of reflector is derived based on the gas film lubrication. After coupled the gas film thickness and Reynolds Equation, the pressure distribution can be acquired by using finite difference methods (FDM). Secondly, the shear force which produced by pressure gradient can be decomposed into reflector. In the meantime, the experimental setup has been built to verify the relationship between eccentricity and restoring force.

2. GOVERNING EQUATION

2.1 Reynolds Equation

For a symmetrical model, which means centers of radiator and reflector are concentric, the reflector will keep equilibrium in horizontal direction. However, in this study, the centers between radiator plate and reflector plate are misaligned. The distance between them is called eccentricity and is defined as e, as shown in Figure 1. In this condition, the reflector will do a damping oscillation in the horizontal direction until it stops at the equilibrium position. In order to simplify the numerical model,

[1] yuanyuan.liu@tum.de

the effect of inclination will be neglected in this study.

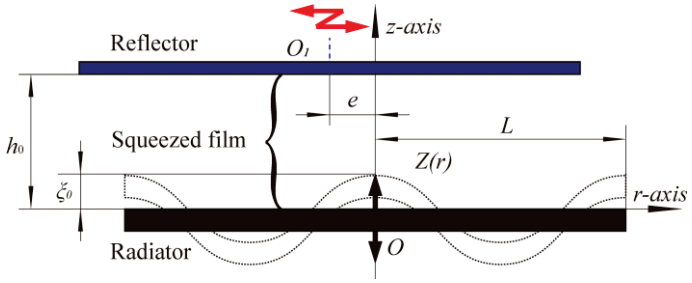

Figure 1 – Misaligned squeeze film model in the cylindrical coordinate

Some assumptions are introduced to simplify the momentum equations. First of all, since the radius of the plate L is considerably greater than the mean thickness of the air film h_0, the pressure gradient in the film thickness direction can be neglected (6). Secondly, this squeeze film is assumed as isothermal film (7). Meantime, the fluid inertia force and body force compared with the viscous force can be neglected in the lower Reynolds number (8). Therefore, the momentum equations in the r- and θ-direction reduced to (9)

$$\begin{aligned}\rho\left(\frac{\partial v_r}{\partial t}\right)&=-\frac{\partial p}{\partial r}+\mu_a\frac{\partial^2 v_r}{\partial z^2}\\ \rho\left(\frac{\partial v_\theta}{\partial t}\right)&=-\frac{1}{r}\frac{\partial p}{\partial \theta}+\mu_a\frac{\partial^2 v_\theta}{\partial z^2}\end{aligned}, \tag{1}$$

where v_r and v_θ are the airflow velocity in the r- and θ-direction, μ_a is the air dynamic viscosity, and ρ, p are the density and pressure of the air in the squeeze film, respectively. Assuming no relative slip between the air and the bottom surface of the reflector, for laminar flow, velocity profile in the r- and θ-directions derived from equation (1) are (10)

$$\begin{aligned}v_r&=\frac{z}{2\mu_a}\frac{\partial p}{\partial r}(z-h)+\dot{u}\frac{z}{h}+\ddot{u}\frac{\rho z}{6\mu_a h}\left(z^2-h^2\right)\\ v_\theta&=\frac{z}{2\mu_a r}\frac{\partial p}{\partial \theta}(z-h)+\dot{\varphi}\frac{zr}{h}+\ddot{\varphi}\frac{\rho z r}{6\mu_a h}\left(z^2-h^2\right)\end{aligned}, \tag{2}$$

where u and φ are the reflector relative horizontal displacement and rotational angle, and h is the film thickness. Combined the airflow velocity expression and the continuity equation, the Reynolds equation in cylindrical coordinate system can be expressed as

$$\begin{aligned}\frac{\partial}{\partial r}\left(rph^3\frac{\partial p}{\partial r}\right)+\frac{1}{r}\frac{\partial}{\partial \theta}\left(ph^3\frac{\partial p}{\partial \theta}\right)&=12\mu_a r\frac{\partial(ph)}{\partial t}+6\mu_a\dot{u}\frac{\partial(rph)}{\partial r}\\ &+6\mu_a\dot{\varphi}\frac{\partial(ph)}{\partial\theta}-\frac{\ddot{u}}{2}\frac{\partial\left(rp\rho h^3\right)}{\partial r}-\frac{\ddot{\varphi}}{2}\frac{\partial\left(p\rho h^3\right)}{\partial\theta}\end{aligned}. \tag{3}$$

2.2 Boundary Conditions

Since the reflector will do a damping oscillation in the horizontal direction, the connection line between O and O_1 can be set as x-axis, as shown in Figure 2. The whole solving domain Ω contains two parts: squeeze domain Ω_s and no squeeze domain Ω_n. The domain Ω is decided by the radius L and closed by boundary $\Gamma(r=L)$. The squeeze domain boundary Γ_s which represented by heavy line in Figure 2 can be expressed by $\Gamma_s\left(r=\sqrt{L^2-(e\cdot\sin\theta)^2}-e\cdot\cos\theta\le L\right)$.

Therefore, the thickness of the air film in squeeze domain can be expressed by

$$h=h_0+\xi_0\cdot Z(r)\cdot\sin(wt), \tag{4}$$

where ξ_0 and $Z(r)$ are the maximum vibration amplitude and mode shape of the radiator in Figure 1, respectively. The pressure in no squeeze domain always equals to the ambient pressure, which means

$$p(\Omega_s)=p_a. \tag{5}$$

The boundary Γ contact with the ambient air means

$$p(\Gamma) = p_a . \tag{6}$$

The pressure gradient at the center O is zero, which means

$$\partial p / \partial r(r = 0, t) = 0 . \tag{7}$$

At the beginning, the reflector plate still placed in the radiator, the film thickness equals zero, and the pressure equals to atmosphere pressure. Thus,

$$p(r, t = 0) = p_a , \; h(r, t = 0) = 0 . \tag{8}$$

Combined the finite difference methods with Newton-Raphson method, the pressure distribution within the solving domain can be obtained (11, 12).

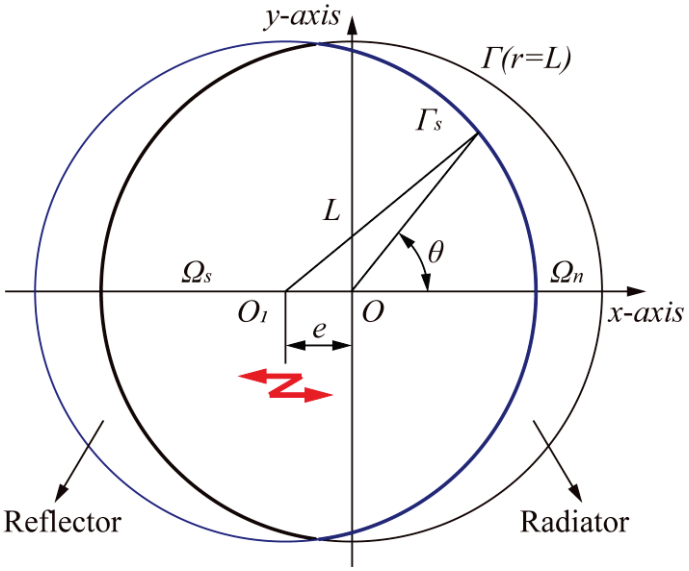

Figure 2 – Schematic diagram of the boundary condition

2.3 Motion Equations

Three types force which caused by squeeze film are applied on reflector: levitation force F_z, horizontal thrust force $F_t = m\ddot{u}$ and rotational moment $M_t = mL^2\ddot{\varphi}/2$. The forces which calculated in the polar coordinate O need to decomposed to polar coordinate O_1, as shown in Figure 3. Since the solving domain and boundary conditions are symmetry about *x*-axis, the pressure distribution will be also symmetric about the *x*-axis. Thus, the rotational moment M_r will equals to zero and thrust force F_t points to positive *x*-direction. Shear stresses τ_{zr} and $\tau_{z\theta}$ are produced by air flow in *r*- and θ-direction acting on a surface normal to the *z*-axis. In the coordinate O_1, both τ_{zr} and $\tau_{z\theta}$ have one component in r_1- and θ_1-direction, respectively. Thus, the thrust force F_t can be expressed by

$$F_t = \int_0^{2\pi}\int_0^L -\left[\tau_{zr}\cos(\theta - \theta_1) + \tau_{z\theta}\sin(\theta - \theta_1)\right] \cdot r\cos(\theta_1) dr d\theta . \tag{9}$$

The position of *N* in coordinate O_1 can be expressed by

$$r_1 = \sqrt{r^2 + e^2 - 2re\cos(\pi - \theta)}, \; \theta_1 = \theta - arcsin\left[e \cdot \sin(\pi - \theta)/r_1\right] . \tag{10}$$

For a Newtonian fluid, combined equation (2) with the shear stresses in the flow acting on a surface normal to the *z*-axis in cylindrical coordinate, the expression for the shear stress on the bottom surface of the reflector are expressed as

$$\begin{aligned} \tau_{zr}\big|_{(z=h)} &= \mu_a \frac{\partial v_r}{\partial z}\Big|_{(z=h)} = \frac{h}{2}\frac{\partial p}{\partial r} + \mu_a \frac{\dot{u}}{h} + \frac{\rho h\ddot{u}}{3} \\ \tau_{z\theta}\big|_{(z=h)} &= \mu_a \frac{\partial v_\theta}{\partial z}\Big|_{(z=h)} = \frac{h}{2r}\frac{\partial p}{\partial \theta} + \mu_a \frac{\dot{\varphi} r}{h} + \frac{\rho h\ddot{\varphi} r}{3} \end{aligned} . \tag{11}$$

Equation (11) shows the shear stress mainly depends on pressure gradient and the relative movement of reflector. The levitation force F_z is the integral of pressure in the solving domain, which is given by

$$F_z = \int_0^{2\pi} \int_0^L (p - p_a) \cdot r dr d\theta . \tag{12}$$

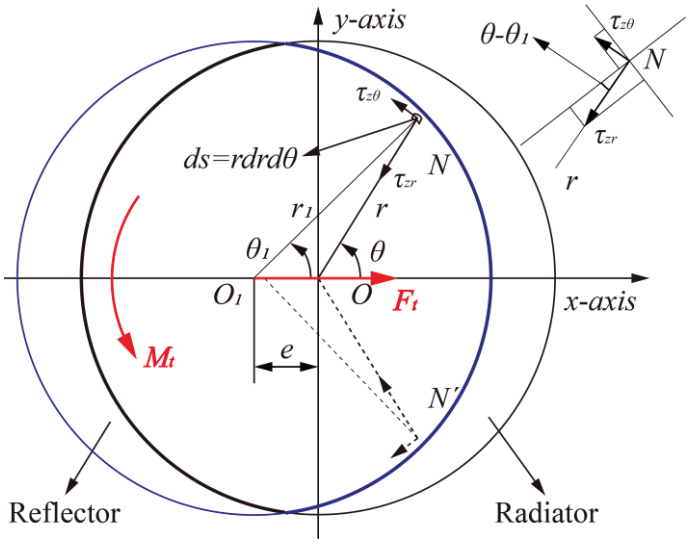

Figure 3 – Geometric diagram for the resolution of shear forces

3. EXPERIMENTAL VALIDATION

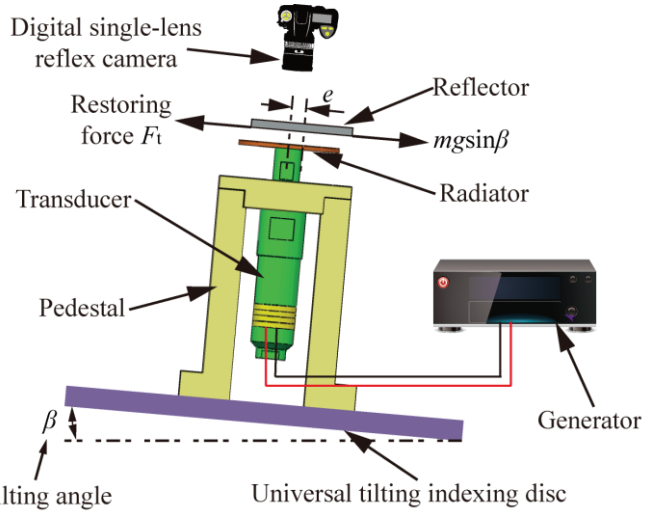

Figure 4 – Schematic diagram of experimental test system

Based on the same transducer and radiator in reference (12), a new reflector plate is used to measure the relationship between eccentricity and restoring force. It made of AL2024 and has the same diameter as radiator which is 120 mm. The thickness and gravity of this plate are 3 mm and 0.9244 N, respectively. Reference the experimental measurement method (13), a universal tilting indexing disc is used to approximately measure the restoring force. A schematic diagram of the experimental setup is shown in Figure 4. It includes a universal tilting indexing disc, transducer and the corresponding control unit, as well as a digital single-lens reflex camera for monitoring the levitation performance of the plate. The transducer was fixed on the universal tilting indexing disc, which can be tilted in a certain angle β by adjusting the control system. Therefore, the eccentricity e is adjusted until the restoring force and the gravity component balanced each other, which means $F_t = mg \sin\beta$.

4. RESULTS

4.1 Pressure Distribution

Figure 5 shows the pressure distribution in radiator coordinate O at the start time of one stable cycle. The excitation amplitude, levitation force and eccentricity are 16 μm, 0.9244 N and 10 mm, respectively. The radiator works in second order vibration mode and the excitation frequency is 19 kHz. Note that the shape of pressure is corresponding with the mode shape in the squeeze domain Ω_s. The reason for this is that the vibration mode shape is one boundary condition to accurate the gas film thickness. If the eccentricity equals to zero, the pressure distribution will be symmetrical in squeeze domain as shown in reference (12) and the reflector will keep stable situation. In the non-squeeze domain Ω_n, the pressure value equals to 1, which means the pressure equals to atmospheric pressure.

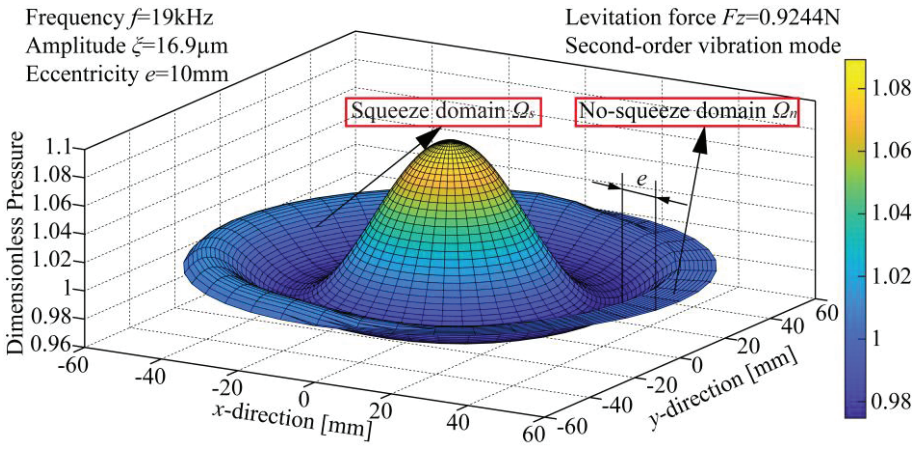

Figure 5 – Pressure distribution in solving domain

4.2 Eccentricity

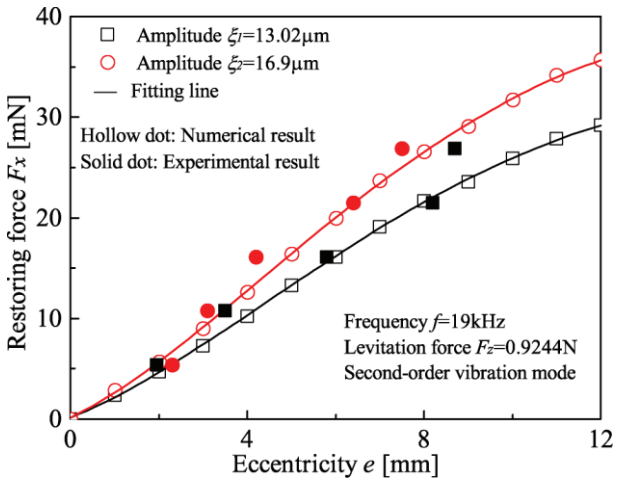

Figure 6 – Comparison of the restoring force versus eccentricity

In general, eccentricity is the most important factor which affect the restoring force distribution. Thus, the influence of the eccentricity e on restoring force is shown in Figure 6. The hollow and solid dot denote the numerical and experimental result, respectively. Notably, the numerical results exhibit reasonably good agreement with the experimental results in lower eccentricity. Since the calculation with the assumption of the inclination of reflector is neglectful. In the lower eccentricity, this assumption is acceptable. However, with the increase of eccentricity, the inclination is a very important factor which affect the stability of reflector. In two different excitation amplitude, the restoring force increases with the increase of eccentricity. It is noted that the increase gradient will be decrease with the eccentricity increases. The same variation tendency has also been reported in reference (3).

5. CONCLUSIONS

This study presents a novel theoretical analysis method for calculating the restoring force based on gas film lubrication theory. At first, an updated Reynolds Equation which considering the movement of reflector is derived. Combined with the levitation height, the pressure distribution can be acquired by using Finite Difference Methods. Secondly, by using the coordinate transformation, the restoring force acting on the reflector can be calculated. Numerical results show that the restoring force increases as the increasing of eccentricity and the relationship between them is nonlinear. Meanwhile, the experimental setup which used to prove this relationship is built. The numerical experimental results show good agreement with the experimental numerical results, which means the method is effective for predict the stability of NFAL system.

ACKNOWLEDGEMENTS

The authors acknowledge the support from China Scholarship Council (CSC) (File No. 201808340068). Meantime, the authors would like to acknowledge Dr. Kai Feng, Professor at Hunan University, China, for valuable suggestions and support on the experiment.

REFERENCES

1. Erzincanli F, Sharp J. M, Erhal S. Design and operational considerations of a non-contact robotic handling system for non-rigid materials. Int J Mach Tool Manu. 1998; 38(4):353-361.
2. Kim O. S, Lee S. H, Han D. C. Positioning performance and straightness error compensation of the magnetic levitation stage supported by the linear magnetic bearing. IEEE T Ind Electron. 2003;50(2):374-378.
3. Hu J. H, Nakamura K, Ueha S. Stability analysis of an acoustically levitated disk. IEEE T Ultrason Ferr. 2003;50(2):117-127.
4. Koike Y, Ueha S, Okonogi A, Amano T, Nakamura K. Suspension mechanism in near field acoustic levitation phenomenon. Ultrason, 2000 IEEE. 2000;1:671-674.
5. Li J, Liu P., Ding H, Cao W. Nonlinear restoring forces and geometry influence on stability in near-field acoustic levitation. J Appl Phys. 2011;109(8):084518.
6. Minikes A, Bucher I. Noncontacting lateral transportation using gas squeeze film generated by flexural traveling waves--numerical analysis. J Acoust Soc Am. 2003;113(5):2464-2473.
7. Minikes A, Bucher I. Coupled dynamics of a squeeze-film levitated mass and a vibrating piezoelectric disc: numerical analysis and experimental study. J Sound Vib. 2003;263(2):241-268.
8. Stolarski T, Chai W. Self-levitating sliding air contact. Int J Mech Sci. 2006;48(6):601-620.
9. Mohite S. S, Sonti V. R, Pratap R. A compact squeeze-film model including inertia, compressibility, and rarefaction effects for perforated 3-D MEMS structures. J Microelectromech S. 2008;17(3):709-723.
10. Gross W. A. Gas film lubrication. New York, USA: Wiley; 1962. p. 17-52.
11. Heshmat H, Walowit J, Pinkus O. Analysis of gas-lubricated foil journal bearings. J. of Lubrication Tech. 1983;105(4):647-655.
12. Li W, Liu Y, Feng K. Modelling and experimental study on the influence of surface grooves on near-field acoustic levitation. TribolL Int. 2017;116:138-146.
13. Koyama D, Nakamura K, Ueha S. A stator for a self-running, ultrasonically-levitated sliding stage. IEEE T Ultrason Ferr. 2007;54(11):2337-2343.